Solar-sail Steering Laws to Calibrate the Accelerations from Solar Radiation Pressure, Planetary Radiation Pressure, and Aerodynamic Drag

Livio CARZANA[a,*], W. Keats WILKIE[b], Andrew HEATON[c], Ben DIEDRICH[c], Jeannette HEILIGERS[a]

[a] *Faculty of Aerospace Engineering, Delft University of Technology, Kluyverweg 1, 2629 HS Delft, The Netherlands*
[b] *Langley Research Center, National Aeronautics and Space Administration, Hampton, Virginia, 23681-2199, USA*
[c] *Marshall Space Flight Center, National Aeronautics and Space Administration, Huntsville, Alabama, 35808, USA*

Abstract

Solar sailing is a propulsion method which takes advantage of solar radiation pressure (SRP) as main source of thrust. However, around Earth, other sources also affect the solar-sail dynamics, including planetary radiation pressure (PRP) and atmospheric drag. In literature, the accelerations from SRP, PRP, and atmospheric drag are modeled using different theoretical and idealistic models, which make use of simplifying assumptions to describe the near-Earth dynamical environment, the sail's geometry, and optical properties. Consequently, sailcraft in orbit experience accelerations different from the theoretically predicted ones. In order to quantify these discrepancies between the real and modeled solar-sail dynamics, a first definition and preliminary assessment of a set of calibration steering laws is provided in this paper. These steering laws allow to characterize the solar-sail acceleration at every sail orientation and to identify the contributions due to solar radiation pressure, planetary radiation pressure, and aerodynamic drag. The analyses presented make use of NASA's upcoming ACS3 mission as baseline scenario and account for different possible orientations of its orbit. The results highlight the benefits and implementation challenges of each steering law and the impact that they have on the orbital elements, with particular focus on the orbital altitude.

Keywords: solar sail, calibration, steering laws, operational constraints, Earth-bound, ACS3 mission

1. Introduction

Solar sailing is a propulsion method using solar radiation pressure (SRP) as primary source of thrust [1]. Over the last years, solar sailing has drawn increasing attention in the scientific community particularly because of its propellantless nature and potential for a variety of mission applications, both in the near-Earth and interplanetary environments [2, 3]. In light of this, several solar sails have been launched in the recent past to increase the solar-sail technology readiness level and assess its potential for real-life mission applications. Most of these sailcraft have flown in close proximity of the Earth and, similarly, even more Earth-bound missions are planned for the near future. Among these are, for example, the recently launched Alpha sailcraft by Gama and the upcoming NASA's Advanced Composite Solar Sail System (ACS3) and Gama's Beta missions [4]. Orbiting about the Earth, the dynamics of these solar sails are, apart from SRP, also affected by other sources of acceleration. The main non-gravitational ones include the Earth's planetary radiation pressure (PRP) and atmospheric drag. Because the PRP and aerodynamic accelerations depend on the sail attitude and can perturb sailcraft orbits to a significant extent [5, 6], accurately predicting their magnitudes is crucial for the design of Earth-bound solar-sail missions. In literature, the accelerations from SRP, PRP, and atmospheric drag are modeled using different theoretical and idealistic models, most of which assume the sail to be a thin, flat surface with known optical properties [1, 7, 8]. These models therefore do not account for secondary effects, like the sail billowing, presence of wrinkles, degradation, and uncertainties in the sail's optical properties. Furthermore, these models make use of simplifying assumptions to describe the near-Earth dynamical environment, particularly with respect to the atmospheric density [5, 9, 10] and the intensity of the solar and planetary radiation [6, 11, 12]. Because of these assumptions, real-life sailcraft generally experience accelerations that differ from the predicted ones. In order to quantify these

* Corresponding author, L.Carzana@tudelft.nl

differences, the calibration of the actual SRP, PRP, and aerodynamic accelerations experienced by sailcraft in orbit can be performed. In this way, these accelerations can be measured and compared to the predicted ones, therefore providing insights into, and an opportunity to improve, the accuracy and fidelity of the solar-sail dynamical models. Calibration of the SRP, PRP, and aerodynamic accelerations requires the definition of steering laws designed ad hoc for this purpose. In addition, the implementation of these control strategies in real life can prove challenging for different reasons, including the presence of operational constraints and deorbiting effect on the sailcraft orbit. In light of the above and the fact that studies on the design of such steering laws have never been conducted, this paper presents a set of calibration steering laws (CSLs) specific for Earth-bound solar sails and provides a first-order assessment of their calibration capacity and implementation challenges.

2. Dynamics

In this paper, the equations of motion describing the solar-sail dynamics are expressed in an inertial Earth-centered reference frame, $\mathcal{I}(x, y, z)$, with the x-axis pointing towards the vernal equinox, the z-axis perpendicular to the equatorial plane and pointing towards the north pole, and the y-axis completing the right-handed frame. Within this frame, the equations of motion of a solar sail subject to the SRP, PRP, aerodynamic, and J_2 gravitational accelerations can be expressed in vectorial form as:

$$\ddot{\boldsymbol{r}} + \frac{\mu}{r^3}\boldsymbol{r} = \boldsymbol{a}_{SRP} + \boldsymbol{a}_{PRP} + \boldsymbol{a}_{Aero} + \boldsymbol{a}_{J2} \tag{1}$$

where μ = 398600.4415 km^{3}s^{-2} is the Earth's gravitational parameter [13], $\boldsymbol{r} = [x, y, z]^{\mathrm{T}}$ is the sailcraft position vector, $r = \|\boldsymbol{r}\|$, and $\boldsymbol{a}_{SRP}$, $\boldsymbol{a}_{PRP}$, $\boldsymbol{a}_{aero}$, and $\boldsymbol{a}_{J2}$ are the SRP, PRP, aerodynamic, and Earth's J_2 gravitational accelerations, respectively. The full definition of these accelerations is provided in the following sections.

2.1. Solar Radiation Pressure Acceleration

The SRP acceleration is computed considering an ideal sail model, that is, the sail is assumed to be flat and perfectly reflecting on both sides. Under this assumption, the SRP acceleration is given as [1]:

$$\boldsymbol{a}_{SRP} = \nu a_c \cos^2(\alpha)\, \kappa \hat{\boldsymbol{n}} \tag{2}$$

In Eq. (2), ν represents the shadow factor, computed using a conservative conical shadow model [5]. This model assumes $\nu = 0$ when the sailcraft is in umbra or penumbra and $\nu = 1$ when the sailcraft is completely illuminated. The characteristic acceleration, a_c, represents the maximum achievable SRP acceleration at a distance of 1 AU from the Sun and is defined as [1]:

$$a_c = \frac{2\mathbb{S}_\oplus}{c\sigma} \tag{3}$$

where $\mathbb{S}_\oplus = 1367$ W/m^2 is the solar flux at Earth [13], $c = 299792.458$ km/s is the speed of light in vacuum [14], and σ represents the sailcraft loading parameter, i.e., its mass-to-sail area ratio. Finally, $\alpha \in [0, \pi]$ is the solar-sail pitch angle measured between the direction of sunlight, $\hat{\boldsymbol{s}}$, and the normal direction of the sail back side, $\hat{\boldsymbol{n}}$, see Fig. 1a, while κ is a sign function indicating whether the sail front side is illuminated ($\kappa = 1$) or the sail back side is illuminated ($\kappa = -1$).

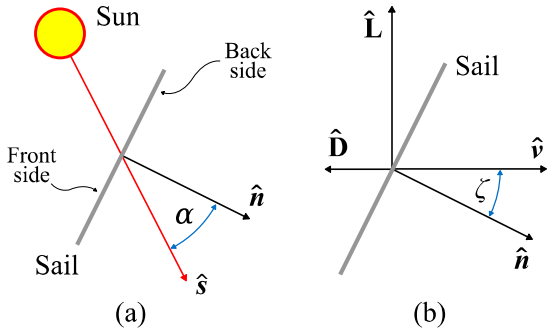

Fig. 1. Relevant solar-sail attitude angles and directions used to determine the SRP and aerodynamic accelerations.

2.2. Aerodynamic Acceleration

The aerodynamic acceleration is computed assuming the sail to behave as a perfectly flat plate in hyperthermal free-molecular flow conditions, that is, the sailcraft is assumed to orbit with a velocity much larger than the thermal velocity of the atmospheric particles [15]. Under these conditions, the aerodynamic acceleration is found as [5, 9]:

$$\boldsymbol{a}_{aero} = \frac{\rho v^2}{2\sigma}(C_D\hat{\mathbf{D}} + C_L\hat{\mathbf{L}}) \tag{4}$$

In Eq. (4), v is the magnitude of the sailcraft inertial velocity and ρ is the atmospheric density, which is modeled using an averaging technique based on the NRLMSISE-00 atmospheric model, see Ref. [5]. $\hat{\mathbf{D}}$ and $\hat{\mathbf{L}}$ represent the drag and lift directions pointing opposite and perpendicular to the inertial velocity direction, $\hat{\boldsymbol{v}}$, respectively, see Fig. 1b. C_D and C_L are the drag and lift coefficients, respectively, given by [5, 9]:

$$C_D = 2\left[\sigma_T + \sigma_N V_R |\cos\zeta| + (2 - \sigma_N - \sigma_T)\cos^2\zeta\right]|\cos\zeta| \tag{5}$$

$$C_L = 2\left[\sigma_N V_R + (2 - \sigma_N - \sigma_T)|\cos\zeta|\right]|\cos\zeta|\sin\zeta \tag{6}$$

where V_R is the ratio of the atmospheric particle thermal velocity to the sailcraft velocity, σ_N and σ_T are the normal and tangential momentum accommodation coefficients, respectively, and ζ represents the complementary angle to the angle of attack, see again Fig. 1b. Based on Ref. [16], in this paper $\sigma_N = \sigma_T = 0.8$ and $V_R = 0.05$.

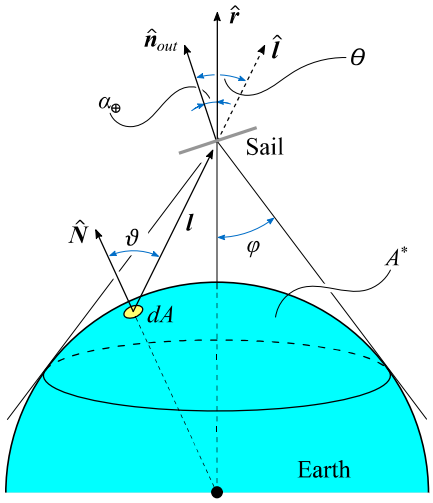

Fig. 2. Geometry of the problem to determine the PRP acceleration exerted on a solar sail.

2.3. *Planetary Radiation Pressure Acceleration*

To compute the PRP acceleration, the so-called spherical uniform model presented in Refs. [6, 17] is employed. This model is valid for flat, perfectly reflecting solar sails and assumes the Earth to be a spherical radiation source emitting radiation isotropically, i.e., with a constant radiation flux. When this model is employed, the PRP acceleration is found through the following integral equation [6, 17]:

$$\boldsymbol{a}_{PRP} = \frac{2\overline{S}}{\pi c \sigma}\left(\int_{A^*} \frac{\cos(\vartheta)\cos^2(\theta)}{l^2} dA\right)\hat{\boldsymbol{n}}_{out} \qquad (7)$$

As depicted in Fig. 2, dA represents an elementary piece of Earth's surface irradiating, ϑ is the angle between the zenith direction at dA, $\hat{\boldsymbol{N}}$, and the vector pointing from dA to the sailcraft, $\boldsymbol{l}$, θ is the angle between $\boldsymbol{l}$ and the sail normal direction pointing away from the Earth, $\hat{\boldsymbol{n}}_{out}$, and $l = \|\boldsymbol{l}\|$. Finally, $\overline{S}$ represents the Earth's planetary flux, which is found through a surface averaging process and is assumed constant over the entire visible surface of the Earth as seen from the sailcraft, A^*. Its value depends on the Earth's blackbody radiation flux and albedo coefficient which, based on Ref. [6], have been set to 234.732 W/m^2 and 0.3259, respectively. For the full analytical expressions of $\overline{S}$ and the solution to the acceleration integral of Eq. (7), the reader is referred to Refs. [6, 17].

2.4. *J_2 Gravitational Acceleration*

The Earth's J_2 gravitational acceleration is defined in frame $\mathcal{G}(x, y, z)$ as follows [18]:

$$\boldsymbol{a}_{J2} = -\frac{3}{2}\frac{R^2}{r^5}\mu J_2\left[(x\hat{\boldsymbol{x}} + y\hat{\boldsymbol{y}})\left(1 - 5\frac{z^2}{r^2}\right) + z\left(3 - 5\frac{z^2}{r^2}\right)\hat{\boldsymbol{z}}\right] \qquad (8)$$

where $\hat{\boldsymbol{x}}$, $\hat{\boldsymbol{y}}$, and $\hat{\boldsymbol{z}}$ are the unit vectors along the $\mathcal{G}(x, y, z)$ frame's axes, $R = 6378.1363$ km is the Earth radius [13], and $J_2 = 1.082626925639 \cdot 10^{-3}$ is the Earth's J_2 gravitational field constant of the JGM-2 geopotential model [13, 19].

3. Calibration Steering Laws

In this section, the definition of a set of steering laws designed to calibrate the SRP, PRP, and aerodynamic accelerations of solar sails in Earth-bound, circular orbits is discussed. To this aim, it is crucial to firstly define the concept of the acceleration envelope (AE) curve: this is a curve representing the set of all possible accelerations achievable by a sailcraft when changing its attitude. Because the SRP, PRP, and aerodynamic accelerations change their magnitudes and directions with the sail attitude, an AE curve can be defined for each of them. When the acceleration models presented in Section 2 are considered, these curves assume the shapes depicted in Fig. 3. As can be seen, all AE curves are symmetric with respect to a different reference direction; these are the sunlight direction, $\hat{\boldsymbol{s}}$, radial direction, $\hat{\boldsymbol{r}}$, and velocity direction, $\hat{\boldsymbol{v}}$, for the SRP, PRP, and aerodynamic AE curves, respectively. The reference directions provide information on which attitudes maximize or minimize a particular acceleration. Indeed, if the sail normal direction, $\hat{\boldsymbol{n}}$, is directed along a reference direction or perpendicular to it, the corresponding acceleration is maximized or minimized, respectively. On the other hand, for arbitrary orientations of $\hat{\boldsymbol{n}}$, intermediate accelerations are obtained whose magnitude and direction are described by the AE curves, see Fig. 3.

Given the notion of AE curve, the CSLs can be regarded as control strategies that solar sails can adopt to reconstruct the AE curves based on the in-orbit accelerations experienced. The difficulty in designing CSLs for the SRP, PRP, and aerodynamic accelerations is the fact that all these accelerations depend on the sail attitude and are therefore coupled. Consequently, in most cases it is not possible to calibrate a single acceleration independently without experiencing a perturbing effect from the others. In addition, it is worth noting that the design

of the CSLs also depends on the relative orientation of the orbit with respect to sunlight, as the presence of eclipses hinders the calibration of the SRP acceleration.

Hereinafter seven CSLs with different degrees of complexity are presented. In Section 3.1, steering laws to calibrate the maximum SRP, PRP, and aerodynamic accelerations are discussed. Afterwards, Section 3.2 presents another three CSLs to calibrate the entire SRP, PRP, and aerodynamic AE curves. Finally, in Section 3.3 a steering law designed to calibrate the residual accelerations acting on solar sails in the absence of SRP, PRP, and aerodynamic accelerations is discussed.

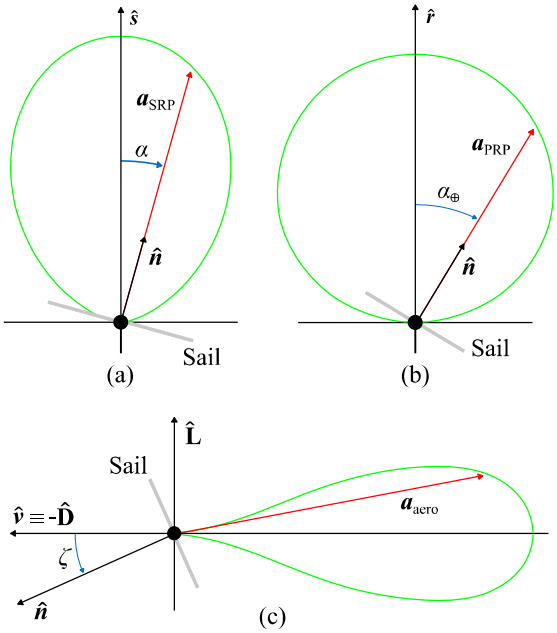

Fig. 3. Acceleration envelope curves of the SRP acceleration (a), PRP acceleration (b), and aerodynamic acceleration (c).

3.1. *Calibration of the Maximum Accelerations*

The steering laws discussed in this section aim to calibrate the maximum magnitudes of the SRP, PRP, and aerodynamic accelerations, therefore allowing to determine the characteristic dimensions of their AE curves. To achieve this, for each of these acceleration a steering law can be designed in which the sail is constantly oriented with its normal parallel to the acceleration's reference direction, that is, $\hat{\boldsymbol{n}}$ points along $\hat{\boldsymbol{s}}$, $\hat{\boldsymbol{r}}$, and $\hat{\boldsymbol{v}}$ when calibrating the maximum SRP, PRP, and aerodynamic accelerations, respectively. This approach can be used to calibrate the maximum PRP and aerodynamic accelerations at any point along the orbit and the maximum SRP acceleration only when the sailcraft is illuminated. Indeed, when the sailcraft is in eclipse conditions ($\nu = 0$), sunlight cannot reach the sailcraft and, therefore, the SRP acceleration cannot be measured. In this case, an alternative control strategy can be adopted: the sail is oriented edgewise with respect to the velocity direction, $\hat{\boldsymbol{v}}$, and with its normal pointing along the radial direction, $\hat{\boldsymbol{r}}$. This configuration minimizes drag, therefore preventing the sail from deorbiting. On the other hand, the PRP acceleration is maximized, hence potentially enabling its calibration. It should be noted that this variant of the CSL is only implemented when eclipses longer than a specified threshold duration, Δt_{Ecl}, take place. The reason for this is that switching to this alternative control strategy requires a sudden re-orientation of the sailcraft, which can prove demanding for real-life attitude control systems. As a consequence, it may be preferable not to implement this variant of the CSL when short eclipses are experienced, despite the perturbations PRP acceleration and drag may yield. In this paper, a value of Δt_{Ecl} equal to 1/5 of the orbital period is considered for all CSLs where applicable.

3.2. *Calibration of the Acceleration Envelope Curves*

This section presents three CSLs that aim to calibrate the entire AE curves of the SRP, PRP, and aerodynamic accelerations.

3.2.1. *Solar Radiation Pressure Acceleration*

In order to calibrate the SRP AE curve, the sailcraft shall to change its attitude gradually, so as to cover all pitch angles in the range 0-90 deg. Depending on whether eclipses occur, two possible control strategies are adopted.

If the sailcraft is continuously illuminated along the entire orbit, the sail's normal direction, $\hat{\boldsymbol{n}}$, points along the sunlight direction, $\hat{\boldsymbol{s}}$, at the point in the orbit closest to the Sun. When moving away from this point, $\hat{\boldsymbol{n}}$ slowly changes its direction so as to increase the pitch angle, until becoming perpendicular to the direction of sunlight and parallel to the radial direction, $\hat{\boldsymbol{r}}$, after one quarter of the orbital period. Thereafter, the sail is gradually reoriented to make $\hat{\boldsymbol{n}}$ be once again parallel to $\hat{\boldsymbol{s}}$ after another quarter of the orbital period. Finally, the entire process is repeated also in the second half of the orbit, thus making the pitch angle span across the 0-90 deg range twice per orbital period.

If eclipses last longer than the specified threshold duration, Δt_{Ecl}, the same eclipsing variant of the CSL presented in Section 3.1 for the calibration of the maximum SRP acceleration can be used. When this variant of the CSL is adopted, the pitch angle spans across the 0-90 deg range only once per orbital period. For the sake of visualization, this variant of the CSL is displayed in the left plot of Fig. 4.

3.2.2. *Planetary Radiation Pressure Acceleration*

When implementing the CSL for the PRP AE curve, the sailcraft gradually changes its attitude by translating its normal direction from $\hat{\boldsymbol{r}}$ to $\pm\hat{\boldsymbol{h}}$ (and vice versa) every quarter of the orbital period. In this way, the planetary cone angle (i.e., the angle between $\hat{\boldsymbol{n}}_{out}$ and $\hat{\boldsymbol{r}}$, see Figs. 3 and 4), $\alpha_{\oplus}$, spans across the entire 0-90 deg range twice per orbit. Implementing this steering law does not yield any aerodynamic drag, thus preventing the sailcraft from deorbiting. On the other hand, the SRP acceleration is present and acts as a perturbing acceleration. For the sake of visualization, this CSL is displayed in the center plot of Fig. 4.

3.2.3. *Aerodynamic Acceleration*

Similar to the CSL presented in the last subsection, the steering law to calibrate the aerodynamic AE curve considers a gradual variation of the sail normal direction between two reference directions: the velocity direction, $\hat{\boldsymbol{v}}$, and the orbital momentum direction, $\hat{\boldsymbol{h}} = (\hat{\boldsymbol{r}} \times \hat{\boldsymbol{v}}) / \|\hat{\boldsymbol{r}} \times \hat{\boldsymbol{v}}\|$. In particular, $\hat{\boldsymbol{n}}$ is continuously re-oriented so as to point intermittently along $\hat{\boldsymbol{v}}$ and $\pm\hat{\boldsymbol{h}}$ every quarter of the orbital period. By doing so, the complementary angle to the angle of attack, ζ, spans across the entire 0-90 deg range twice per orbit. When employing this CSL, no PRP acceleration is experienced by the sailcraft, whereas the SRP acceleration acts as a perturbing acceleration. For the sake of visualization, this CSL is displayed in the right plot of Fig. 4.

3.3. *Calibration of the Residual Accelerations*

Solar sails experience no SRP, PRP, and aerodynamic accelerations when the sail normal direction, $\hat{\boldsymbol{n}}$, points perpendicular to the sunlight direction, $\hat{\boldsymbol{s}}$, radial direction, $\hat{\boldsymbol{r}}$, and velocity direction, $\hat{\boldsymbol{v}}$, respectively. The relative orientation of $\hat{\boldsymbol{s}}$, $\hat{\boldsymbol{r}}$, and $\hat{\boldsymbol{v}}$ then plays a central role in determining whether a zero-acceleration steering law can be designed. The only scenario in which all three accelerations can be simultaneously nullified is when $\hat{\boldsymbol{s}}$, $\hat{\boldsymbol{r}}$, and $\hat{\boldsymbol{v}}$ are coplanar. This only occurs for an orbit oriented parallel to the direction of sunlight. Then, the sail normal direction, $\hat{\boldsymbol{n}}$, can be directed perpendicular to the orbital plane, i.e., along $\pm\hat{\boldsymbol{h}}$. Because the SRP, PRP, and aerodynamic accelerations are equal to zero when this CSL is employed, only gravitational accelerations affect the dynamics. However, in the majority of orbital scenarios, these directions do not lie in the same plane and, therefore, a sail normal direction that is perpendicular to all of them is not possible to find. This implies that at least one non-zero acceleration is always obtained, independently of the sail attitude adopted.

4. Analyses

This section presents different analyses aimed at highlighting the benefits and implementation challenges of the CSLs introduced in the previous section. Indeed, while the CSLs can be used to successfully determine a sailcraft's achievable accelerations, their implementation also entails a number of operational difficulties to be taken into account. Among these, five are deemed of particular importance:

- Altitude decrease. Implementing the CSLs can yield considerable changes in the sailcraft's orbital parameters. Among these, the most significant is the decrease in orbital altitude, which is particularly evident for steering laws yielding a large aerodynamic drag.
- Solar-sail attitude rate of change. Some CSLs require rapid changes of attitude which can prove demanding for the attitude control system of the sailcraft.
- Exposure of the sail's back side to sunlight. Solar sails usually consist of a polymer film membrane covered with an aluminum coating on the front side in order to enhance reflectivity. Since the sail's back side is generally not illuminated, it is either left uncoated or has a chromium coating, so as to increase the sail's emissivity for thermal control [1, 20]. However, some CSLs allow the sail's back side to be

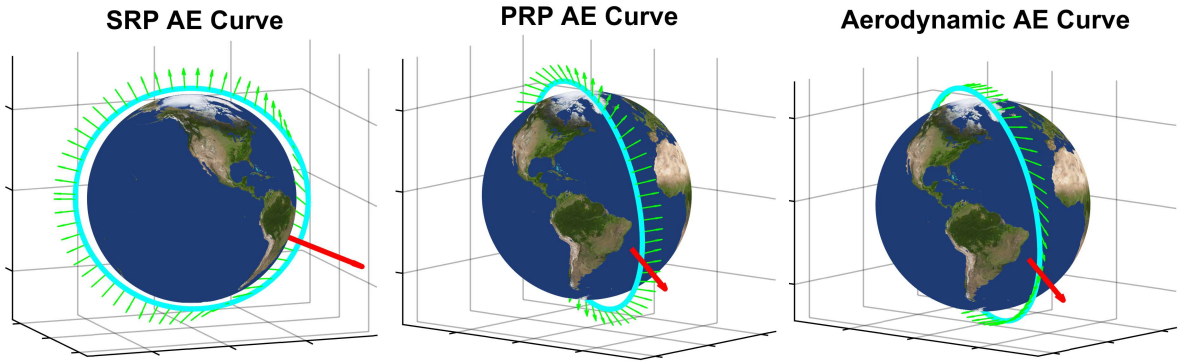

Fig. 4. Steering laws to calibrate the SRP, PRP, and aerodynamic AE curves for the ACS3 sailcraft orbit with local time of the ascending node at 12AM. The light blue curve, red arrow, and green arrows indicate the sailcraft orbit, Earth-to-Sun direction, and sail normal directions, respectively.

exposed to sunlight. When this occurs, ultraviolet radiation yields a rapid degradation of the sail material and its optical properties. It should be noted that since in this paper a double-coated, perfectly reflecting solar sail is considered, see Section 2.1, this degradation effects are not accounted for in the dynamics. Nevertheless, the analyses presented later in this section will provide insights on the frequency of exposure of the sail's back side to sunlight, so as to quantify its potential effect on real-life solar-sail missions to a first-order extent.

- Exposure of the sail's back side to the ram direction. In addition to sunlight, the sail's back side can experience rapid degradation also when exposed to the ram direction, i.e., the direction of motion. This is due to the effect of atomic oxygen, which deteriorates the sail's back side material upon impact, creating cracks in the polymer/chromium film. Although the dynamical model used in this paper does not account for these degradation effects, see Section 2, the analyses presented later in this section will provide insights on the frequency of exposure of the sail's back side to the ram direction, so as to quantify its potential effect on real-life sailcraft missions to a first-order extent.
- Power generation. In this paper, it is assumed that solar cells are mounted on the sailcraft in a plane parallel to the sail membrane, i.e., the solar cells generate power when the sail's front side is illuminated. Conversely, no power is produced when the sailcraft is oriented edgewise with respect to the direction of sunlight nor when its back side is exposed. Although these conditions can be endured for short periods of time, some CSLs require prolonged periods of times in which the sail attitude is such that the solar arrays are not exposed to sunlight, thus implying potential power issues.

The analyses presented in this section make use of NASA's ACS3 mission as baseline scenario, with a characteristic acceleration of $a_c = 0.045$ mm/s^2 and the following vector of initial orbital elements defined in frame $\mathcal{G}(x, y, z)$:

$$\left[a_0, e_0, i_0, \Omega_0, \omega_0, f_0\right]^T = \left[7093.1363 \text{ km}, 0, 98.249 \text{ deg}, \begin{Bmatrix} 157.328 \\ 202.328 \\ 247.328 \end{Bmatrix} \text{deg}, 0 \text{ deg}, 0 \text{ deg}\right]^T \quad (9)$$

where a_0, e_0, i_0, Ω_0, ω_0, and f_0 represent the initial orbit's semi-major axis, eccentricity, inclination, right ascension of the ascending node (RAAN), argument of pericenter, and true anomaly, respectively. The orbital elements in Eq. (9) identify a circular, Sun-synchronous orbit with an initial altitude of $h_0 = a_0 - R = 715$ km. In order to consider different orbit orientation with respect to sunlight, three values of the RAAN are considered, which correspond to local times of the ascending node (LTANs) at 6AM, 9AM, and 12AM. For each of these initial orbits and each CSL presented in Section 3, the dynamics given in Eq. (1) have been propagated using Matlab®'s *ode45* integrator, with absolute and relative tolerances set to 10^{-12}. The analyses consider a simulation start date of December 1st, 2023 (i.e., the expected deployment date of the sail) and a simulation duration of 10 days. Finally, to account for realistic solar-sail attitude-change capabilities, the CSLs have been implemented considering the ACS3 sailcraft's maximum attitude rate of change (RoC), equal to 0.5 deg/s.

Table 1 presents the results of the analyses for each combination of initial LTAN and CSL. In order to provide insights into the calibration of the target acceleration and perturbing effects of the other accelerations, the three columns on the left-hand side of the table specify the extent to which each AE curve is covered when employing a specific CSL. The acceleration to be calibrated (referred to as "calibration target") is displayed in bold, while the perturbing accelerations are given in brackets. Here, the terms "Max" and "Zero" indicate that a particular acceleration is constantly equal to its maximum achievable value or zero, respectively. Similarly, in the case a CSL covers a larger portion of the AE curve, the terms "Full", "Intermediate", and "Minor" are given, which indicate that the calibration target/perturbing AE curve is covered completely, partially, or only to a minor extent. The right-hand side of the table provides information on the operational difficulties introduced at the beginning of this section. Here, the altitude loss due to implementing the given CSL for 10 days, Δh, is shown, as well as the maximum attitude RoC. To quantify the effect the CSLs have on the degradation of the sail, two columns are added which provide the percentage of orbital period during which the sail's back side is exposed to sunlight and the ram direction. In a similar fashion, to measure the effect each steering law has on the sailcraft power-generation capabilities, the percentage of orbital period during which the sail's front side is exposed to sunlight with a pitch angle smaller than 80 deg is given. Finally, to enable a qualitative overview of the benefits and drawbacks of each CSLs, a color code has been applied to the data of Table 1, with green representing benefits and yellow, orange, and red indicating potential issues of increasing degree of severity.

As can be seen in the table, calibration of the maximum SRP acceleration and its AE curve can prove challenging due to multiple reasons. To begin with, the sailcraft experiences significant perturbations from the aerodynamic and PRP accelerations for increasing values of the initial LTAN, which lead to moderate decreases in altitude in the range 7.6-12.1 km. Furthermore,

Table 1. Calibration capabilities and implementation challenges of the calibration steering laws for different initial LTANs.

CSL	Initial LTAN	**Calibration Target** (Perturbation)			Δh [km]	Max. Attitude RoC [deg/s]	Sail's Back Side Exposure [% orbital period]		Solar Cells' Exposure to Sunlight ($\alpha \leq 80$ deg) [% orbital period]
		SRP Acc.	PRP Acc.	Aerodyn. Acc.			Sunlight	Ram direction	
Max. SRP Acc.	6 AM	**Max**	(Minor)	(Minor)	7.656	0	0	50	83.18
	9 AM	**Max**	(Intermediate)	(Intermediate)	9.736	0.5	0	36.08	68.21
	12 AM	**Max**	(Full)	(Full)	12.106	0.5	0	34.23	64.34
Max. PRP Acc.	6 AM	(Minor)	**Max**	(Zero)	0.013	0.061	50	0	21.87
	9 AM	(Intermediate)	**Max**	(Zero)	0.016	0.061	50	0	11.27
	12 AM	(Full)	**Max**	(Zero)	0.012	0.061	50	0	08.75
Max. Aerodyn. Acc.	6 AM	(Minor)	(Zero)	**Max**	36.985	0.061	41.63	0	36.00
	9 AM	(Intermediate)	(Zero)	**Max**	36.705	0.061	34.06	0	30.61
	12 AM	(Full)	(Zero)	**Max**	36.440	0.061	32.21	0	29.27
SRP AE Curve	6 AM	**Full**	(Full)	(Intermediate)	8.379	0.061	0	50	71.99
	9 AM	**Full**	(Full)	(Intermediate)	8.308	0.061	0	25	55.60
	12 AM	**Full**	(Full)	(Full)	9.282	0.061	0	25	53.24
PRP AE Curve	6 AM	(Full)	**Full**	(Zero)	0.006	0.086	50	0	28.93
	9 AM	(Intermediate)	**Full**	(Zero)	0.013	0.086	50	0	14.13
	12 AM	(Intermediate)	**Full**	(Zero)	0.007	0.086	48.36	0	08.41
Aerodyn. AE Curve	6 AM	(Full)	(Zero)	**Full**	17.961	0.096	41.63	0	39.53
	9 AM	(Intermediate)	(Zero)	**Full**	19.193	0.086	34.07	0	32.13
	12 AM	(Intermediate)	(Zero)	**Full**	19.594	0.086	32.05	0	21.70
Residual	12 AM	**Zero**	**Zero**	**Zero**	0.002	0	0	0	0

exposure of the sail's back side to the ram direction for long periods of time also occurs and, for the maximum SRP acceleration CSLs, a large attitude RoC may also be required. The CSLs for the maximum aerodynamic and PRP accelerations present common challenges due to the significant perturbation from SRP (especially for larger initial LTANs) and the prolonged exposure of the sail's backside to sunlight. Both these CSLs imply potential power issues, as the sail's front side is exposed to sunlight only for a limited time. This is particularly evident when calibrating the maximum PRP acceleration, as the sail has its front side constantly facing the Earth, therefore allowing little sunlight to illuminate it. The CSL for the maximum aerodynamic acceleration, on the other hand, presents another major disadvantage, that is, the deorbiting effect on the orbit. This happens because drag is maximized, therefore yielding a rapid loss in altitude in the order of 36 km. It should be noted that this large value of Δh is also due to the simulation start time considered. Indeed, because on December 1st, 2023 high solar activity is expected, the atmospheric density is high and, therefore, aerodynamic drag is significant. The steering laws to calibrate the PRP and aerodynamic AE curves present potential problems similar to the CSLs for the maximum PRP and aerodynamic accelerations. Large perturbations by the SRP are experienced and, once again, the sail's backside is exposed to sunlight frequently. The CSL for the PRP AE curve also yields short time windows in which the solar cells can generate power, whereas, on the other hand, the CSL for the aerodynamic AE curve yields large altitude loss, in the order of 19 km. The results in Table 1 also highlight an interesting property of the PRP and aerodynamic accelerations, that is, their orthogonality. Indeed, because the analyses in this section consider circular initial orbits, the radial and velocity directions are roughly perpendicular at all times during the propagations. This implies that it is always possible to design CSLs for which the PRP or aerodynamic acceleration is varied while the other is left unchanged. Because of this, in Table 1 the steering laws to calibrate the aerodynamic acceleration show that PRP never perturbs the dynamics. In a similar fashion, for the CSLs for the PRP acceleration, aerodynamic drag is always equal to zero. Finally, the CSL to quantify the residual accelerations only implies one major operational challenges, that is, the fact that sunlight never illuminates the sail's front side and no power can be generated. This is due to the particular attitude of the sail, which is constantly oriented edgewise with respect to sunlight. It is also worth noting that, to implement this CSL, the sail must be oriented edgewise also with respect to the velocity and the radial directions. These three conditions can be met only if an initial LTAN at 12AM is considered, which is the reason for which no simulation has been performed for this CSL with LTANs at 6AM and 9AM.

Although the operational constraints given in Table 1 may render the adoption of the CSLs more challenging, it should be noted that they do not necessarily constitute killer requirements for the implementation of these control strategies. For example, the CSLs requiring a large attitude RoC of 0.5 deg/s may be implemented allowing for a slower re-orientation of the sail when entering the eclipse region, so as to

decrease the attitude RoC and, therefore, the effort required by the sailcraft attitude control systems. Furthermore, even though exposure of the sail's back side to the ram direction and/or sunlight has a detrimental effect on the sail's material, it should be noted that these situations may be endured for a certain period of time, thus still allowing for the calibration of the solar-sail accelerations. In a similar fashion, CSLs that involve a large loss of altitude or inability to generate power may also be implemented for short periods of time. Nevertheless, because these constraints are deemed the most severe, implementing CSLs that entail loss of altitude and inability to generate power may only be possible for sailcraft with sufficiently large characteristic accelerations and energy storage capacities.

5. Conclusions

This paper provided a first-order investigation on strategies to calibrate the accelerations experienced by real-life solar sails in Earth-bound orbits, with particular focus on the solar radiation pressure (SRP), planetary radiation pressure (PRP), and aerodynamic accelerations. To quantify the maximum magnitude of these accelerations and their variation with the sail attitude, several calibration steering laws (CSLs) have been presented. Also, to assess the calibration capabilities of these steering laws, several analyses have been conducted using NASA's upcoming ACS3 mission as baseline scenario. The results show that the calibration of the SRP acceleration is more easily achieved for dawn-dusk sun-synchronous orbits than for other sun-synchronous orbits, as in the former case the PRP and aerodynamic accelerations affect the dynamics less severely. Indeed, for noon-midnight orbits, the PRP and aerodynamic accelerations produce larger perturbations which render the calibration process more challenging. Similarly, when the CSLs for the PRP and aerodynamic accelerations are employed, SRP represents a source of disturbance which hinders their calibration, regardless of the orbit's orientation. The analyses performed also highlighted practical implementation challenges of the CSLs. Indeed, it was found that the CSLs for the SRP acceleration can require rapid changes of attitude, which may prove challenging for the sailcraft's attitude control system. Furthermore, these CSLs also entail a prolonged exposure of the sail's back side to incoming atmospheric particles, which accelerates the sail's material degradation. Sail degradation also takes place when the CSLs for the PRP and aerodynamic accelerations are employed, as the sail's back side is often exposed to sunlight. Implementing these steering laws also entails potential issues for power generation, as the sailcraft's solar arrays are hardly exposed to sunlight along the orbit. Finally, it was found that the most challenging CSLs for orbital stability are the ones to calibrate the aerodynamic acceleration, as significant drag is generated during calibration and rapid altitude losses are achieved, even in the order of 3.6 km per day. Altitude loss and inability to generate power are considered the most crucial constraints that can hinder the implementation of the CSLs. As a consequence, the CSLs for the PRP and aerodynamic accelerations are deemed the most challenging to implement, whereas the CSL for the SRP acceleration proves to be more easily implementable.

References

[1] C. R. McInnes, Solar Sailing - Technology, Dynamics and Mission Applications, Springer, 2004.

[2] D. A. Spencer, L. Johnson and A. C. Long, "Solar sailing technology challenges," *Aerospace Science and Technology,* vol. 93, 2019. DOI: 10.1016/j.ast.2019.07.009.

[3] M. Macdonald and C. R. McInnes, "Solar Sail Science Mission Applications and Advancement," *Advances in Space Research,* pp. 1702-1716, 2011. DOI: 10.1016/j.asr.2011.03.018.

[4] W. K. Wilkie, J. M. Fernandez, O. R. Stohlman and et al., "An Overview of the NASA Advanced Composite Solar Sail (ACS3) Technology Demonstration Project," *AIAA Scitech 2021 Forum,* 2021.

[5] L. Carzana, P. Visser and J. Heiligers, "Locally optimal control laws for Earth-bound solar sailing with atmospheric drag," *Aerospace Science and Technology,* vol. 127, no. 107666, 2022. DOI: 10.1016/j.ast.2022.107666.

[6] L. Carzana, P. Visser and J. Heiligers, "A New Model for the Planetary Radiation Pressure Acceleration for Solar Sails," *under review at the Journal of Guidance, Control, and Dynamics,* 2023.

[7] B. Wie, "Solar Sail Attitude Control and Dynamics, Part 1," *Journal of Guidance, Control, and Dynamics,* vol. 27, no. 4, pp. 526-535, 2004.

[8] M. Macdonald, Advances in Solar Sailing, Springer, 2014, pp. 95-113.

[9] V. Stolbunov, M. Ceriotti, C. Colombo and C. R. McInnes, "Optimal Law for Inclination Change in an Atmosphere Through Solar Sailing," *Journal of Guidance, Control, and Dynamics,* vol. 36, no. 5, pp. 1310-1323, 2013. DOI: 10.2514/1.59931.

[10] G. Mengali and A. A. Quarta, "Near-Optimal Solar-Sail Orbit-Raising from Low Earth Orbit," *Journal of Spacecraft and Rockets,* vol. 42, no. 5, pp. 954-958, 2005. DOI: 10.2514/1.14184.

[11] A. Barles, M. Ceriotti, F. Ciampa and L. Felicetti, "An Optimal Steering Law for Sailing with Solar and Planetary Radiation Pressure," *Aerospace Science and Technology,* vol. 118, 2021. DOI: 10.1016/j.ast.2021.107051.

[12] A. De Iuliis, F. Ciampa, L. Felicetti and M. Ceriotti, "Sailing with Solar and Planetary Radiation Pressure," in *Proceedings of ISSS 2019: 5th International Symposium on Solar Sailing*, Aachen, Germany, 2019. DOI: 10.1016/j.asr.2019.11.036.

[13] J. R. Wertz and W. J. Larson, Space Mission Analysis and Design, El Segundo: Microcosm Press and Dordrecht: Kluwer Academic Publishers, 2005.

[14] E. Tiesinga, P. J. Mohr, D. B. Newell and B. N. Taylor, "CODATA recommended values of the fundamental physical constants: 2018," *Reviews of Modern Physics,* vol. 93, 2021. DOI: 10.1103/RevModPhys.93.025010.

[15] J. A. Storch, "Aerodynamic Disturbances on Spacecraft in Free-Molecular Flow," The Aerospace Corporation, 2002.

[16] P. C. Hughes, Spacecraft Attitude Dynamics, New York: Dover Publications Inc., 2004.

[17] L. Carzana, P. Visser and J. Heiligers, "A New Model for the Planetary Radiation Pressure Acceleration for Solar Sails," in *2022 AAS/AIAA Astrodynamics Specialist Conference [AAS 22-715]*, Charlotte, North Carolina, United States of America, 2022.

[18] K. F. Wakker, Fundamentals of Astrodynamics, Delft, The Netherlands: Delft University of Technology, Institutional Repository, 2015.

[19] R. S. Nerem et al., "Gravity Model Development for TOPEX/POSEIDON: Joint Gravity Models 1 and 2," *Journal of Geophysical Research,* vol. 99, no. C12, pp. 24,421-24,447, 1994. DOI: 10.1029/94JC01376.

[20] J. Ho Kang et al., "Durability characterization of mechanical interfaces in solar sail membrane structures," *Advances in Space Research,* vol. 67, no. 9, pp. 2643-2654, 2021.